Magnetic structure and anisotropy of [Co/Pd][subscript 5]/NiFe multilayers

Magnetic structure and anisotropy of $[Co/Pd]_5$/NiFe multilayers

Larysa Tryputen,[1,*] Feng Guo,[2,3] Frank Liu,[1] T. N. Anh Nguyen,[4,5] Majid S. Mohseni,[4,6] Sunjae Chung,[4,7] Yeyu Fang,[7] Johan Åkerman,[4,7,8] R. D. McMichael,[2] and Caroline A. Ross[1]

[1]*Department of Materials Science and Engineering, MIT, Cambridge, Massachusetts 02139, USA*
[2]*Center for Nanoscale Science and Technology, National Institute of Standards and Technology, Gaithersburg, Maryland 20899, USA*
[3]*Maryland Nanocenter, University of Maryland, College Park, Maryland 20742, USA*
[4]*Materials and Nano Physics Department, School of ICT, Royal Institute of Technology (KTH), Stockholm-Kista 16440, Sweden*
[5]*Spintronics Research Group, Laboratory for Nanotechnology (LNT), Vietnam National University, Ho Chi Minh City, Vietnam*
[6]*Department of Physics, Shahid Beheshti University, G.C., Evin, Tehran 19839, Iran*
[7]*Department of Physics, University of Gothenburg, 41296 Gothenburg, Sweden*
[8]*NanOsc AB, Electrum 205, 16440 Kista, Sweden*

(Received 9 September 2014; revised manuscript received 29 November 2014; published 9 January 2015)

The magnetization behavior, magnetic anisotropy, and domain configurations of Co/Pd multilayers with perpendicular magnetic anisotropy capped with permalloy is investigated using magnetometry, magnetic force microscopy, and ferromagnetic resonance. The thickness of the $Ni_{80}Fe_{20}$ layer in $[Co/Pd]_5$/NiFe (t) was varied from $t = 0$ to 80 nm in order to study the interplay between the anisotropy and magnetization directions of Co/Pd and NiFe. By varying the thickness of the NiFe layer, the net anisotropy changes sign, but domains with plane-normal magnetization are present even for the thickest NiFe. Ferromagnetic resonance measurements show a decrease in damping with increasing NiFe thickness. The results demonstrate how the magnetic behavior of mixed-anisotropy thin films can be controlled.

DOI: 10.1103/PhysRevB.91.014407 PACS number(s): 75.30.Gw, 75.60.−d, 76.50.+g, 75.78.Cd

I. INTRODUCTION

Magnetic multilayers with strong perpendicular magnetic anisotropy and exchange-spring structures consisting of high-anisotropy multilayers coupled with soft magnetic films have been extensively studied due to their interesting fundamental properties and promising technological applications. Multilayers formed from thin alternating ferromagnetic and nonmagnetic materials such as Co/Pd, Co/Pt, and Fe/Pt or two ferromagnetic materials such as Co/Ni exhibit high perpendicular anisotropy originating from the interfaces [1–4]. The static and dynamic properties in such multilayer films have been studied in detail (Co/Pd, Co/Pt [5,6], [Co/Pd]/Fe[Co/Pd] [7], Co/Ni [4,8], CoNi/Pt [9], CoFe/Pd [10], and CoFe/Ni [11]). High-anisotropy films are attractive for nonvolatile memory, logic, and other spin torque based devices because they impart high thermal stability, scalability, and low critical current for current-induced magnetization switching and domain wall motion [12,13], and they can support surface magnetic drops (dissipative solitons) which may have an impact on domain wall electronics [14,15].

Coupling the high-anisotropy multilayer with a soft layer allows wide control over the magnetic properties of the composite film by adjusting the layer composition, layer thicknesses, number of repeats, and interfacial anisotropy. There have been several studies of systems with mixed anisotropies where the exchange coupling can be used to tailor the magnetic properties ([Co/Pd]-NiFe [16,17], [Co/Pd]-Co-Pd-NiFe [18], [Co/Ni]-NiFe [19], $[Co/Pd]_8$-NiFe [20], [Co/Pd]-CoFeB [21], and CoCrPt-Ni [22]). Exchange-spring films are being pursued for nanoscale spin transfer torque oscillators whose frequency is tunable over a wide range by modifying the injected spin polarized current [23–25]. The damping parameter of the materials is also relevant to spintronic applications. Magnetic films with high-Z atoms often have very strong spin-orbit interactions and high damping [26], and many materials with perpendicular anisotropy containing Pt also have a high damping constant, with typically [26] $\alpha = 0.05$–0.1. However, materials with only low-Z elements often have low spin-orbit coupling and low damping, such as CoFeB with $\alpha = 0.001$–0.01. A low damping constant α reduces the critical current for switching [13], but the damping constant has been found to increase with the anisotropy in high-anisotropy materials and in composite structures such as [Co/Pd]/Fe/[Co/Pd] [7,13].

These results illustrate the importance of the damping parameter and the interplay between anisotropies in governing the magnetic properties of composite films made from a high-anisotropy multilayer coupled to a soft layer. In this article, we investigate the role of the soft layer on the magnetic anisotropy, domain structure, and damping in exchange-coupled $[Co/Pd]_5$/NiFe films. The results are extended to a wider range of NiFe layer thicknesses, from 3 to 80 nm, compared with previous studies [16,17,19]. Also, we characterize damping and anisotropy by ferromagnetic resonance measurements, and domain structure by magnetic imaging and simulation. We find that the effective anisotropy changes sign as the NiFe thickness is near 6 nm, but domains are present even for thick NiFe due to coupling with the Co/Pd multilayer. The damping decreases as the NiFe thickness increases. The static and dynamic magnetic properties and domain configuration can therefore be tailored by varying the thickness of the NiFe layer.

II. EXPERIMENTAL METHODS

The films were grown onto Si(100) substrates by dc magnetron sputter deposition in a chamber with

*tryputen@mit.edu

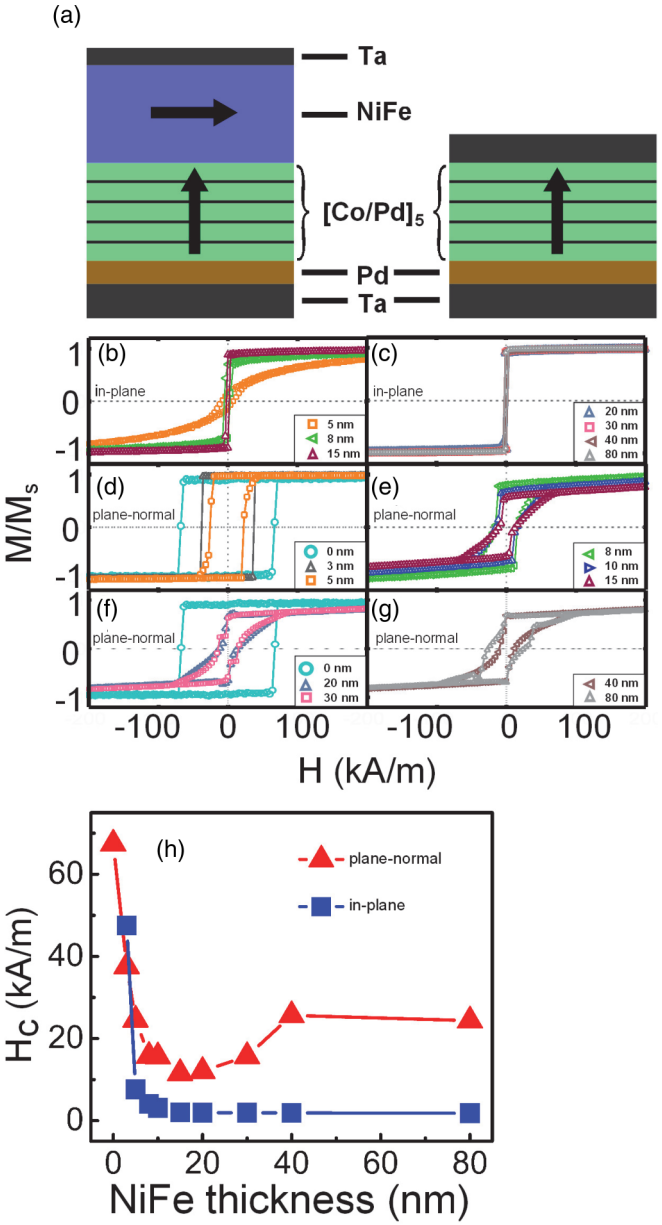

FIG. 1. (Color online) (a) Schematic illustration of exchange-coupled Ta/Pd/$[Co/Pd]_5$/NiFe/Ta multilayer structure. The film consists of NiFe with in-plane anisotropy and $[Co/Pd]_5$ with high perpendicular anisotropy. (b)–(g) Experimental in-plane and plane-normal hysteresis loops of perpendicular $[Co/Pd]_5$/NiFe, $t = 0$–80 nm. (h) Evolution of the coercive field H_c as a function of the NiFe layer thickness.

a base pressure below 4×10^{-6} Pa (3×10^{-8} Torr) at ambient temperature. The multilayers consisted of Ta(5 nm)/Pd(3 nm)/[Co(0.5 nm)/Pd(1 nm)]$_5$/NiFe(t nm) /Ta (5 nm), where the thicknesses of all single layer films were determined by x-ray reflectometry and the film thicknesses of each layer in the final stacks were estimated from the deposition rate and deposition time. The Co/Pd multilayer was the same for each film, but the thickness t of the NiFe varied between 0 and 80 nm [Fig. 1(a)]. The thin amorphous Ta seed layer allows for greater mobility of the deposited atoms and an improved fcc-(111) orientation of the Pd layer deposited upon it, thus improving the perpendicular anisotropy of the [Co/Pd] multilayers [16,27].

Samples were characterized by vibrating sample magnetometry (VSM), magnetic force microscopy (MFM), and ferromagnetic resonance spectroscopy (FMR). The in-plane and plane-normal magnetic hysteresis loops were measured by VSM. A diamagnetic signal from the sample holder and uncoated substrate was subtracted, and the loops were normalized by the moment at 870 kA/m. Magnetic domains were imaged by MFM after ac plane-normal demagnetization and at remanence after applying a saturating (870 kA/m) normal or in-plane magnetic field. CoCr low-moment probes were used in order to minimize the influence of the stray field from the probe on the multilayers. FMR measurements were performed using a wide coplanar waveguide and a lock-in technique. The width of the signal line was about 600 μm. All measurements were performed at ambient temperature.

III. RESULTS AND DISCUSSION

A. Hysteresis loops and domain structure

The in-plane and plane-normal hysteresis loops for samples of $[Co/Pd]_5$/NiFe (t nm) with t ranging from 0 to 80 nm are given in Figs. 1(b)–1(g), demonstrating the magnetization reorientation transition. The measured in-plane and plane-normal coercivities H_c are plotted as a function of NiFe thickness in Fig. 1(h).

The saturation magnetization increased with NiFe film thickness as the film volume increasingly consisted of NiFe ($Ni_{80}Fe_{20}$: $M_s = 8 \times 10^5$ A/m) [28] compared with Co/Pd ($M_s = 3.7 \times 10^5$ A/m) [17]. In the absence of a NiFe layer, and for NiFe thicknesses of 3 or 5 nm, the $[Co/Pd]_5$ exhibited a square hysteresis loop and in-plane hard axis, but for samples with a NiFe layer of 8 nm thickness or above, the in-plane loop showed a low coercivity and abrupt switching, and plane-normal loops had a slow approach to saturation. The magnetic easy axis therefore reorients from plane normal to in plane for NiFe between 5 and 8 nm. The plane-normal loops in Figs. 1(d) and 1(e) reveal a significant remanence and the samples with a NiFe thickness of 0–5 nm could be saturated below 100 kA/m. The remanence shows a clear decreasing trend for samples with a NiFe layer of 5–15 nm thickness, which is in an agreement with our previous studies [16].

Figure 2 shows MFM images after ac demagnetization in a plane-normal field. In the demagnetization process the magnetic field was cycled to zero with decreasing amplitude in 0.1% steps from about 12×10^6 A/m, producing a demagnetized state. From Fig. 2(e), the sample without NiFe and with 3 nm NiFe showed micron-sized domains with a strong contrast at the domain walls. Thicker samples formed stripe domains in a labyrinth pattern with a period 250 nm for $t = 20$ nm and a period 200 nm for $t = 40$ and 80 nm. The strong perpendicular anisotropy of the $[Co/Pd]_5$ multilayer that was exchange coupled to the NiFe layer produced a domain contrast that was visible even for thick NiFe layers.

Figure 3 shows remanent states for samples with 20, 30, and 80 nm NiFe after both in-plane and plane-normal saturation. The 20 nm NiFe sample showed dendritelike domains at

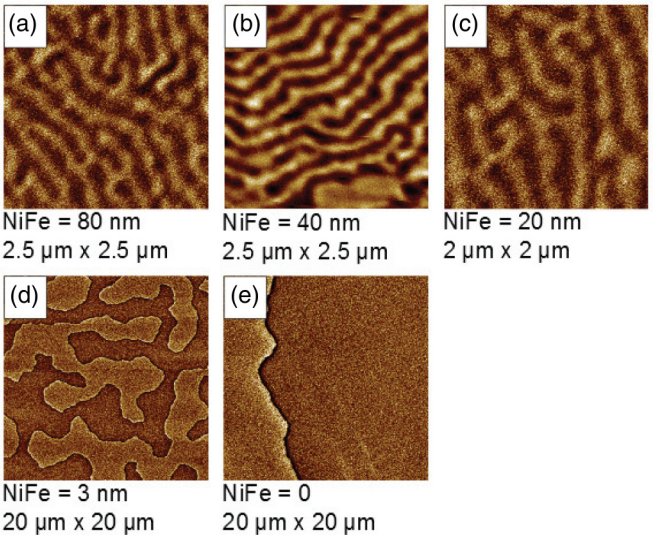

FIG. 2. (Color online) MFM phase images from the domain structure of $[Co/Pd]_5$/NiFe multilayers after plane-normal ac demagnetization for the multilayers with different thicknesses of NiFe, as indicated below the plots. The color scale represents degrees of phase in the range 1°–1.3°.

remanence after plane-normal saturation with a period 300 nm and more angular boundaries than in the ac-demagnetized case. The 30 nm NiFe sample showed similar angular domains at remanence after in-plane saturation. The sample with an 80 nm thick NiFe layer showed weaker contrast stripe domains at remanence after plane-normal saturation with a period 400 nm and a poorly ordered domain structure at remanence after in-plane saturation.

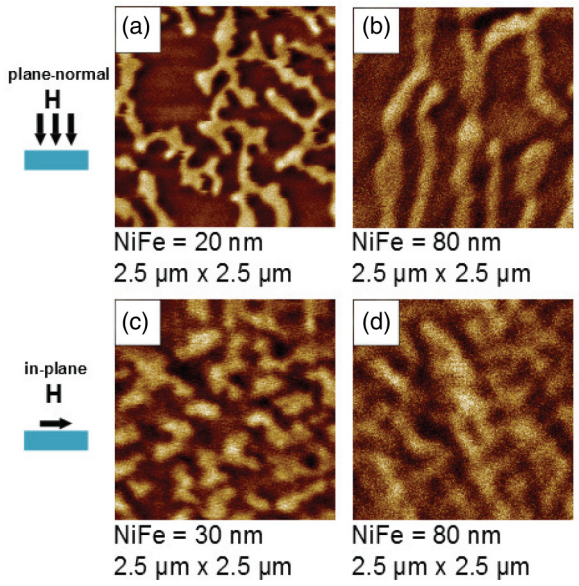

FIG. 3. (Color online) Remanent magnetic domain structures by MFM imaging after (a), (b) plane-normal and (c), (d) in-plane saturation for $[Co/Pd]_5$/NiFe multilayers with NiFe of (a) 20 nm, (c) 30 nm, and (b), (d) 80 nm thickness. The color scale represents degrees of phase in the range 1°–1.3°.

To show whether the stripe domains were intrinsic to the NiFe film, MFM images were also taken for a single, continuous, 80 nm thick NiFe film after ac demagnetization in a plane-normal field. The image was featureless and did not reveal any domain structure. We therefore conclude that the domain patterns are due to the presence of the $[Co/Pd]_5$ multilayer [20], leading to a perpendicular component of magnetization even in NiFe with a thickness over ten times that of the 7.5 nm thick $[Co/Pd]_5$.

It is worth mentioning that there is a relation between remanence measured from VSM hysteresis loops and MFM images. From the remanent MFM images after plane-normal saturation [Fig. 3(a) for $[Co/Pd]_5$/NiFe 20 nm and Fig. 3(b) for $[Co/Pd]_5$/NiFe 80 nm], the areas of the dark regions of the MFM phase images are 35% for $t = 20$ nm and 46% for $t = 80$ nm, corresponding to a remanence of 0.6 and 0.4, respectively, if the domain contrast represents regions with a plane-normal magnetization direction. However, in the hysteresis loops of Figs. 1(f) and 1(g), the remanence is close to 0.5. The difference may be a result of a through-thickness variation in the magnetization orientation, since the MFM is more sensitive to magnetization at the top surface whereas the VSM averages the magnetization throughout the volume.

In prior modeling [16], the NiFe magnetization was tilted towards the film plane with increasing distance from the interface. The tilt reached 60° for a NiFe thickness of 8 nm. The current MFM results show that even in thicker films there remains a significant plane-normal magnetization component near the top surface of the NiFe. The presence of the [Co/Pd] multilayer therefore profoundly affects the domain structure in the NiFe via exchange coupling.

B. Micromagnetic modeling

The OOMMF micromagnetic code [29] was used to model the remanent magnetization configuration of the $[Co/Pd]_5$/NiFe samples with different NiFe thicknesses $t = 4$, 20, and 80 nm (Fig. 4). The model included a NiFe layer that was exchange coupled to a $[Co/Pd]_5$ layer at the bottom surface of the NiFe film (the x-y plane at a height $z = 0$). The $[Co/Pd]_5$ magnetization was oriented in the plane-normal direction to model stripe domains of a width 100 nm along the y direction. Periodic boundary conditions in the x direction were used to model an infinite array of Co/Pd stripe domains. The NiFe magnetization was initially randomized with an in-plane random vector field, and was then allowed to equilibrate at zero applied field.

Standard values of the magnetic saturation of the soft NiFe layer, $M_s = 8 \times 10^5$ A/m, and the anisotropy, $K_s = 0$ J/m^3, were used. The exchange stiffness in the soft layer, $A^s_{ex} = 13$ pJ/m, was taken from literature [17]. The cell size was 4 nm × 4 nm × 4 nm, so the thinnest NiFe film modeled was 4 nm thick. The sample size in the y direction was set to 1 μm to minimize boundary effects. Perpendicular anisotropy of the $[Co/Pd]_5$ film, $K_h = 6.3 \times 10^5$ J/m^3, was obtained from VSM measurements on a $[Co/Pd]_5$ film, and $A^h_{ex} = 6$ pJ/m [17]. The exchange between the soft and hard layers was modeled with an intermediate value $A^{s\text{-}h}_{ex} = 9.5$ pJ/m. The damping parameter was set at $\alpha = 0.5$ to lead to rapid convergence of the magnetization state.

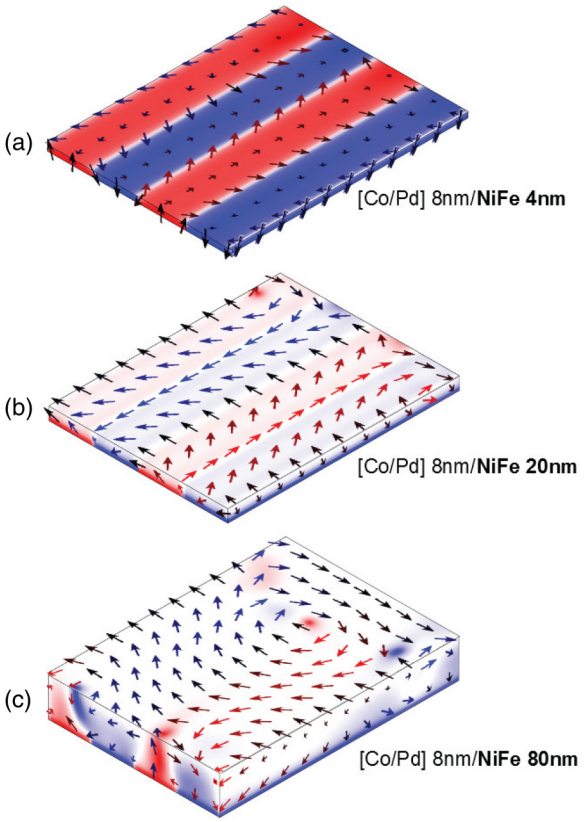

FIG. 4. (Color online) Micromagnetic modeling of the magnetic structure, the cross section at the middle of the multilayer and top view, for the $[Co/Pd]_5$/NiFe t multilayers with (a) $t = 4$ nm, (b) 20 nm, and (c) 80 nm. The colors represent the z component of the magnetization. The lower two layers of cells correspond to $[Co/Pd]_5$.

Figure 4 shows how the remanent magnetization configuration of the NiFe changes with increasing thickness of the NiFe. Figures 4(a)–4(c) shows cross sections in the x-z plane perpendicular to the stripe domains and the top surface of the NiFe. In the cross sections, the arrows represent the projection of the magnetization vectors onto the image plane, with red and black indicating the component along z or $-z$, respectively. In the top view, red and blue represent the magnetization component in the z direction, normal to the film plane. This is the component primarily responsible for contrast in the MFM images.

Figure 4(a) shows clear perpendicular domains in the NiFe corresponding to the domains in the Co/Pd. The domain walls in the NiFe propagate through its thickness, though the magnetization tilts to lie in plane at the top surfaces of the walls, forming Néel caps. For the 80 nm thick NiFe film [Fig. 4(c)], the walls in the NiFe were less vertical, and the magnetization pattern at the top surface of the film was not a direct replica of that of the Co/Pd domains. Nonetheless, the presence of a domain structure at the top surface of the 80 nm thick NiFe film is in good agreement with the contrast seen in MFM images (Figs. 2 and 3). The modeling therefore shows that in the case of the thinnest NiFe layer, $t = 4$ nm, the $[Co/Pd]_5$/NiFe t multilayer retains a high plane-normal remanence, whereas increasing t allows an in-plane component of the magnetization to develop in the NiFe while still retaining a plane-normal component of the NiFe magnetization that is related to the Co/Pd domain structure.

C. FMR measurements

To quantitatively study the effective anisotropy, plane-normal ferromagnetic resonance (FMR) measurements were carried out for $[Co/Pd]_5$/NiFe(t) samples with varying NiFe thicknesses $t = 3, 5, 8, 10$, and 20 nm. An in-plane microwave frequency field was generated using a coplanar waveguide. An external magnetic field was applied along the plane normal. In this configuration, the resonance frequency and applied field follow a linear relation and the effective perpendicular anisotropy field is also obtained from the FMR measurements, as described by the following equation:

$$f = \frac{\mu_0 \gamma}{2\pi}(H_{\text{app}}^{\perp} + H_{\text{eff}}^{\perp}), \tag{1}$$

where f is the resonance frequency, γ is the gyromagnetic ratio, and $H_{\text{app}}^{\perp}$ is the out-of-plane applied field. $H_{\text{eff}}^{\perp}$ is the effective perpendicular anisotropy field, and $H_{\text{eff}}^{\perp} = (2\mu_0 K_{\text{eff}}^{\perp}/M_s) - M_s$, with $K_{\text{eff}}^{\perp}$ being the perpendicular anisotropy.

Figure 5(a) shows the microwave pumping frequency as a function of the resonance field. For all samples measured, the resonance field varied linearly with the microwave pumping frequency, following Eq. (1). The linewidth of the resonance peaks was also measured as a function of frequency, shown in Fig. 5(b). To extrapolate the damping parameter, we fit the linewidth $\mu_0 \Delta H$ with

$$\Delta H = \Delta H_0 + \frac{2\alpha}{\mu_0 \gamma}(2\pi f), \tag{2}$$

where ΔH_0 is a constant indicating the inhomogeneous linewidth broadening, and α is the damping parameter.

Before we discuss the FMR results, we point out that at low frequencies, the applied field is not sufficient to saturate the

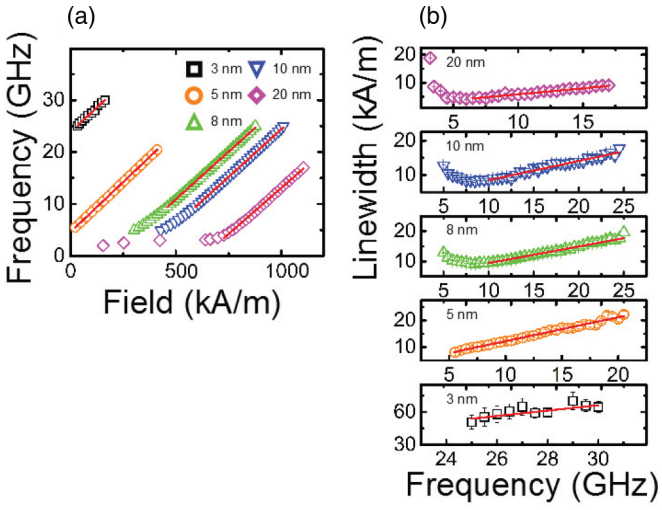

FIG. 5. (Color online) (a) FMR frequency as a function of resonance field, and (b) linewidth dependence on frequency for $[CoPd]_5$/NiFe (t) nm. The standard deviations of the fits are smaller than the data markers.

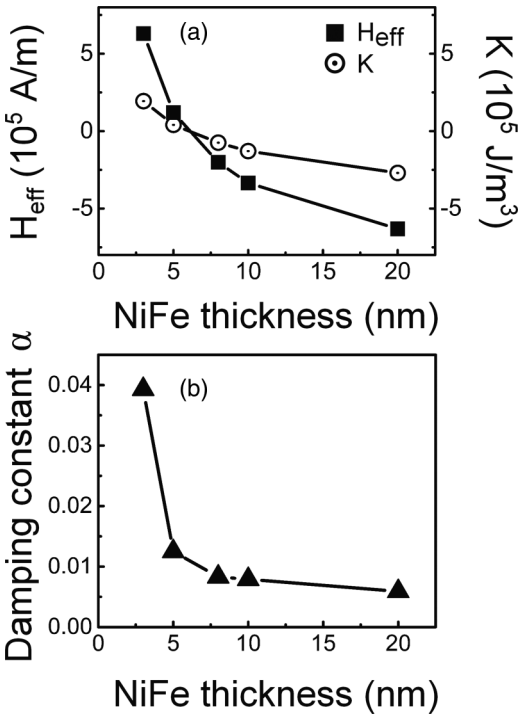

FIG. 6. (a) Dependence of the effective perpendicular anisotropy field $H_{\text{eff}}^{\perp}$ and anisotropy constant K on the thickness of the NiFe layer and (b) damping constant α as a function of the thickness of NiFe. Standard deviations of the fits are smaller than the data symbols.

magnetization and the macrospin analysis of Eq. (1) does not apply in this regime. $f(H_{\text{app}}^{\perp})$ deviates away from the linear relation at lower fields. Furthermore, the enhanced linewidth at low frequencies is also seen in Fig. 5(b) for $t = 5$, 10, and 20 nm, implying an unsaturated magnetization state.

Now we show that the preferred anisotropy orientation depends on the NiFe thickness, in agreement with the magnetometry measurements. The effective perpendicular anisotropy field $H_{\text{eff}}^{\perp}$ and the damping parameter α are shown as a function of NiFe layer thickness, shown in Fig. 6. An anisotropy constant K was calculated from the effective anisotropy field from the relation $K = \mu_0 M_s H_{\text{eff}}^{\perp}/2$, with M_s calculated as a volume weighted average of M_s of NiFe and Co/Pd.

For $t \leqslant 6$ nm, $H_{\text{eff}}^{\perp} > 0$, indicating a plane-normal anisotropy, while for $t \geqslant 8$ nm, $H_{\text{eff}}^{\perp} < 0$, indicating an in-plane anisotropy. Figure 6 also shows the dependence of the damping parameter on the NiFe thickness. For the $t = 20$ nm sample, $\alpha = 0.0059 \pm 0.0002$, a typical value for high quality permalloy films [30]. For a thinner NiFe layer, the influence of the Co/Pd multilayer becomes important and the damping parameter increases rapidly with reducing the NiFe thickness, especially in the out-of-plane anisotropy regime. For $t = 3$ nm, $\alpha = 0.039 \pm 0.01$, nearly seven times larger than that in the 20 nm sample.

It is clear that the anisotropy evolves from plane-normal to in-plane orientation as the thickness of the NiFe layer increased, passing through zero at $t \approx 6$ nm. The FMR measurements are in agreement with hysteresis loops (Fig. 1) and confirm that for the thinnest NiFe layers, $t = 3$ and 5 nm, a net perpendicular anisotropy dominates due to strong coupling between the soft and hard layers. Both the static and dynamic behavior of the thin NiFe samples are largely influenced by the [Co/Pd] multilayer in this regime. Samples with thicker NiFe layers ($t \geqslant 8$ nm) behave more easy-plane-like, because the shape anisotropy energy per unit area increases with thickness while the interlayer coupling energy per unit area is fixed.

IV. CONCLUSIONS

In summary, the static and dynamic magnetic properties of exchange-coupled $[CoPd]_5$/NiFe multilayers are investigated. The anisotropy of the $[CoPd]_5$/NiFe multilayer depends strongly on the thickness of the NiFe layer, and by varying the NiFe thickness, the easy axis can be reoriented from plane normal to in plane. There was a clear trend in anisotropy constant from $(1.94 \pm 0.10) \times 10^5$ J/m^3 at $t = 3$ nm to $(-2.70 \pm 0.14) \times 10^5$ J/m^3 at $t = 20$ nm NiFe, and the damping constant changed between 0.039 ± 0.010 and 0.0059 ± 0.0002 [30]. With increasing NiFe thickness, the morphology of the domain pattern varied from large domains to stripe domains, but even for thick NiFe there was a plane-normal magnetization component at the top surface of the NiFe controlled by the domain pattern in the Co/Pd.

These results expand our understanding about material systems with mixed anisotropies, and indicate that the damping parameter and net anisotropy can be tuned for spintronics applications by using multilayers with mixed anisotropies. For instance, in a spin torque nano-oscillator, the free layer requires small damping constants, low saturation magnetization, small volume, and high polarization to be set in motion by small critical current, whereas a fixed polarizer layer requires a large magnetization, large damping, and large effective field so that the current is not sufficient to cause precession of the polarizer [13]. It is expected that further investigation of such exchange-spring systems such as [Co/Ni]/NiFe [19] could help to realize more effective spin torque oscillators based on high-anisotropy materials in films where both fixed and free layers would take advantage of tilted magnetization.

ACKNOWLEDGMENTS

This work was supported by C-SPIN, one of six STARnet Centers of SRC supported by MARCO and DARPA, the Göran Gustafsson Foundation, National Science Foundation, and Skolkovo Tech. This work made use of the MRSEC Shared Experimental Facilities at MIT, supported by the National Science Foundation under Award No. DMR-08-19762, and in part at the Center for Nanoscale Systems (CNS), a member of the National Nanotechnology Infrastructure Network (NNIN), which is supported by the National Science Foundation under NSF Award No. ECS-0335765. CNS is part of Harvard University. F.G. acknowledges support under the Cooperative Research Agreement between the University of Maryland and the National Institute of Standards and Technology Center for Nanoscale Science and Technology, Award No. 70NANB10H193.

[1] P. F. Carcia, J. Appl. Phys. **63**, 5066 (1988).
[2] J. I. Hong, S. Sankar, A. E. Berkowitz, and W. F. Egelhoff, Jr., J. Magn. Magn. Mater. **285**, 359 (2005).
[3] C. Feng, X. Mei, M. Yang, N. Li, Y. Jiang, G. Yu, and F. Wang, J. Appl. Phys. **109**, 063918 (2011).
[4] S. Fukami, H. Sato, M. Yamanouchi, S. Ikeda, and H. Ohno, Appl. Phys. Express **6**, 073010 (2013).
[5] K. A. Seu, R. Su, S. Roy, D. Parks, E. Shipton, E. E. Fullerton, and S. D. Kevan, New J. Phys. **12**, 035009 (2010).
[6] K. Yakushiji, T. Saruya, H. Kubota, A. Fukushima, T. Nagahama, S. Yuasa, and K. Ando, Appl. Phys. Lett. **97**, 232508 (2010).
[7] J. Dou, M. J. Pechan, E. Shipton, N. Eibagi, and E. E. Fullerton, J. Appl. Phys. **113**, 17C115 (2013).
[8] J. M. Shaw, H. T. Nembach, and T. J. Silva, J. Appl. Phys. **108**, 093922 (2010).
[9] S. Sindhu, M. Haast, K. Ramstck, L. Abelmann, and J. Lodder, J. Magn. Magn. Mater. **238**, 246 (2002).
[10] J. M. Shaw, H. T. Nembach, and T. J. Silva, Phys. Rev. B **85**, 054412 (2012).
[11] J. M. Shaw, H. T. Nembach, and T. J. Silva, Appl. Phys. Lett. **99**, 012503 (2011).
[12] S. Mangin, D. Ravelosona, J. A. Katine, M. J. Carey, B. D. Terris, and E. E. Fullerton, Nat. Mater. **5**, 210 (2006).
[13] S. Ikeda, K. Miura, H. Yamamoto, K. Mizunuma, H. D. Gan, M. Endo, S. Kanai, J. Hayakawa, F. Matsukura, and H. Ohno, Nat. Mater. **9**, 721 (2010).
[14] S. M. Mohseni, S. R. Sani, J. Persson, T. N. Anh Nguyen, S. Chung, Y. Pogoryelov, and J. Åkerman, Phys. Status Solidi RRL **5**, 432 (2011).
[15] Y. Bespyatykh, I. Dikshtein, and S. Nikitov, Phys. Lett. A **184**, 198 (1994).
[16] T. N. A. Nguyen, Y. Fang, V. Fallahi, N. Benatmane, S. M. Mohseni, R. K. Dumas, and J. Åkerman, Appl. Phys. Lett. **98**, 172502 (2011).
[17] S. Tacchi, T. N. A. Nguyen, G. Carlotti, G. Gubbiotti, M. Madami, R. K. Dumas, J. W. Lau, J. Åkerman, A. Rettori, and M. G. Pini, Phys. Rev. B **87**, 144426 (2013).
[18] T. A. Nguyen, N. Benatmane, V. Fallahi, Y. Fang, S. Mohseni, R. Dumas, and J. Åkerman, J. Magn. Magn. Mater. **324**, 3929 (2012).
[19] S. Chung, S. M. Mohseni, V. Fallahi, T. N. A. Nguyen, N. Benatmane, R. K. Dumas, and J. Åkerman, J. Phys. D: Appl. Phys. **46**, 125004 (2013).
[20] G. Heldt, M. T. Bryan, G. Hrkac, S. E. Stevenson, R. V. Chopdekar, J. Raabe, T. Thomson, and L. J. Heyderman, Appl. Phys. Lett. **104**, 182401 (2014).
[21] T. N. A. Nguyen, R. Knut, V. Fallahi, S. Chung, Q. Tuan Le, S. M. Mohseni, O. Karis, S. Peredkov, R. K. Dumas, C. W. Miller, and J. Åkerman, Phys. Rev. Appl. **2**, 044014 (2014).
[22] D. Navas, J. Torrejon, F. Béron, C. Redondo, F. Batallan, B. P. Toperverg, A. Devishvili, B. Sierra, F. Castaño, K. R. Pirota, and C. A. Ross, New J. Phys. **14**, 113001 (2012).
[23] W. H. Rippard, A. M. Deac, M. R. Pufall, J. M. Shaw, M. W. Keller, S. E. Russek, G. E. W. Bauer, and C. Serpico, Phys. Rev. B **81**, 014426 (2010).
[24] S. Russek, W. Rippard, T. Cecil, and R. Heindl, in *Handbook of Nanophysics* (CRC Press, Boca Raton, FL, 2010), pp. 1–23.
[25] D. Houssameddine, U. Ebels, B. Delaet, B. Rodmacq, I. Firastrau, F. Ponthenier, M. Brunet, C. Thirion, J.-P. Michel, L. Prejbeanu-Buda *et al.*, Nat. Mater. **6**, 447 (2007).
[26] A. V. Khvalkovskiy, D. Apalkov, S. Watts, R. Chepulskii, R. S. Beach, A. Ong, X. Tang, A. Driskill-Smith, W. H. Butler, P. B. Visscher *et al.*, J. Phys. D: Appl. Phys. **46**, 074001 (2013).
[27] R. Law, R. Sbiaa, T. Liew, and T. C. Chong, Appl. Phys. Lett. **91**, 242504 (2007).
[28] G. Nahrwold, J. M. Scholtyssek, S. Motl-Ziegler, O. Albrecht, U. Merkt, and G. Meier, J. Appl. Phys. **108**, 013907 (2010).
[29] M. J. Donahue and D. G. Porter, in *Interagency Report NISTIR 6376* (National Institute of Standards and Technology, Gaithersburg, MD, 1999).
[30] Uncertainties quoted in this paper are one standard deviation of the fit parameters.